Ultra Long-Lived Electron-Hole Separation within Water-Soluble Colloidal ZnO Nanocrystals: Prospective Applications for Solar Energy Production

Anna M. Cieślak,[a,†] Mariia V. Pavliuk, [b,†] Luca D'Amario, [b,†] Mohamed Abdellah, [b,†] Kamil Sokołowski,[a] Urszula Rybinska,[b] Daniel L. A. Fernandes,[b] Michał K. Leszczyński,[a] Fikret Mamedov,[b] Ahmed M. El-Zhory,[b] Jens Föhlinger,[b] Alena Budinská,[b] Małgorzata Wolska-Pietkiewicz,[c] Leif Hammarström,[b] Janusz Lewiński[a,c,*] and Jacinto Sá[a,c,*]

[a] *Institute of Physical Chemistry, Polish Academy of Sciences, Warsaw, 01-224, Poland*
[b] *Department of Chemistry, Ångström Laboratory, Uppsala University, Uppsala, 75120, Sweden*
[c] *Faculty of Chemistry, Warsaw University of Technology, Warsaw, 00-661, Poland*

* jacinto.sa@kemi.uu.se; lewin@ch.pw.edu.pl
† These authors contributed equally to the manuscript

Abstract:

Zinc oxide was one of the first semiconductors used in dye-sensitized solar cells but its instability in aqueous media precludes its use for large-scale applications. Herein, we report on a novel ZnO nanocrystal material derived by an organometallic approach that is simultaneously stable and soluble in water due to its carboxylate oligoethylene glycol shell strongly anchored to the inorganic core by the head groups. The resulting unique inorganic core-organic shell interface also stabilizes the photo-generated hole, leading to a dramatic slowing down of charge recombination, which otherwise is a major hurdle in using nanostructured ZnO.

1. Introduction:

Conventional energy resources have been depleted to a great extent by the continuously rising in energy demand. Therefore, it is necessary to find economically viable fuel alternatives that can fulfill the energy and environmental requirements. Solar energy plays an important role both in the generation of electricity and flues. The most promising technologies employ semiconductors to attain robust large-scale solar energy production devices [1]. Thus, understanding electron transfer and dynamics from light harvesting to energy generation is essential. Conceptually a good device has fast electron injection from the photosensitizer into the semiconductor conduction band and slow back electron transfer, in order to have a net gain of charge required for the production of electricity or fuel via photo-catalysis [2,3].

Among the abundant, economic and environmentally friendly semiconductors, both TiO_2 and ZnO are the preferred ones by the emerging technologies primarily due to their electronic [4]. In comparison to TiO_2 anatase, ZnO possesses a significantly higher electron mobility, which favours electron transport across its structures [5]. This property is equally advantageous and disadvantageous since it simultaneously promotes charge separation and recombination. Notably, ZnO nanocrystals (NCs) can form a plethora of morphologies, such as nanowires, nanorods, nanotubes, tetrapods, nanoflowers, nanosheets, and branched nanostructures providing materials of good quality with high surface area via relatively convenient synthetic pathways [6]. However, a significant drawback that so far has precluded large-scale application of ZnO is its poor chemical stability observed in both aqueous acidic and basic media, which stems from its amphoteric behaviour. The use of polymers, *e.g.* polyethylene glycol (PEG), for stabilization and transfer of semiconducting nanostructures to water is an option to overcome these impediments [7]. Interestingly, it has also long been recognized that polymeric agents can significantly affect the optical properties of the parent semiconducting NCs [8]. The effects of this influence are strongly dependent on the nature of both inorganic and the organic components as well as the applied preparation methods. However, these relationships and contribution of different processes to the changes in optical properties remain essentially elusive [9].

Recently, we have developed a novel organometallic approach that can be applied for the synthesis of highly processable carboxylate ligand-coated ZnO NCs [10], including water-soluble ZnO NCs stabilized by a carboxylate oligoethylene glycol (OEG-carboxylate) [10d]. We also showed that the resulting ZnO NCs could be utilized for reversible light-modulation of

supramolecular nanoparticulate systems mediated by photo generation of radical species [10b]. This type of high-quality ZnO material was therefore selected as a suitable platform for further dye-functionalization and investigation of electronic properties relevant to solar energy applications. Herein, we report on detailed spectroscopic characterization of ZnO NCs that are simultaneously stable and soluble in water due to a OEG-carboxylate shell. We also show that the resulting unique inorganic core-organic shell interface works as a hole stabilizer, which dramatically slows down charge recombination process.

2. Experimental:

All reagents were purchased from commercial vendors (Sigma Aldrich and ABCR GmbH) and used as received. Water-soluble ZnO NCs were prepared according to the recently developed organometallic synthetic approach [10d]. For the synthesis we employed 2,5,8,11-tetraoxatetradecan-14-oic acid (MeO-EG_3-COOH; denoted as OEG-H) as oligoethylene glycol proligand, which formed the carboxylate stabilizing shell of ZnO-OEG NCs as depicted in Fig. 1a. Precursor solution (S1) was prepared in –78 °C by mixing of Et_2Zn (1 mmol, 124 mg) in THF (5 mL) with 2 mL of 1 M water solution in THF. The S1 was then brought from -78 °C to -15 °C and stirred for 2 hours. The resulting mixture was then warmed up to 25 C and stirred for further 12 hours. After this time 1 mL of 2,5,8,11-tetraoxatetradecan-14-oic acid stock solution (0.15 M) was added. The resultant mixture was then stirred for further 7 days to produce well-dispersed ZnO-OEG NCs. After evaporation of THF, ZnO-OEG NCs were readily dispersed into water. The water-solubility and stability, morphology as well as organic shell composition of ZnO-OEG NCs was confirmed by dynamic light scattering (DLS), HRTEM (High-resolution transmission electron microscopy), PXRD (powder X-ray diffraction), IR as well as optical measurements (Supporting Information (SI)).

In a separate experiment ZnO-OEG NCs were sensitized with betanin, a natural organic dye [11], yielding the surface modified ZnO-OEG-B NCs (Fig. 1a and 1d). 40 mg of ZnO-OEG NCs were dispersed in DMSO (1 mL) and 1 ml of betanin stock solution (0.092 M) was added to produce betanin functionalized ZnO-OEG-B NCs. The core morphology, hydrodynamic diameter as well as organic shell composition of ZnO-OEG-B NCs were characterized by HRTEM, DLS, IR and ^{1}H NMR spectroscopy (SI). The data indicate that betanin is bound to the NCs' surface and the surface modification did not affect the core size and its crystallinity (SI). Moreover, according to

our expectations, the average hydrodynamic diameter of ZnO-OEG-B slightly increased to 13 ± 2 nm (SI). The ability of ZnO-OEG NCs to undergo betanin sensitization was further confirmed by comprehensive spectroscopic measurements (SI).

Water stability experiments of ZnO-OEG NCs were carried out by the addition of 50μL of a water solution of ZnO-OEG NCs (20 mg/mL) to 2 mL of a HCl or NaOH water solution with pH range of 1-14. For the pH lower than 3.0 and higher than 9.0 gradual sedimentation of highly luminescent precipitate was observed. Therefore, further UV-Vis and DLS measurements were conducted for the samples in the pH range of 3.0-9.0.

Advanced time-resolved experiments were carried out on laser based spectroscopy, with laser powers equating to less than one photon absorption per particle, i.e., no multi-photon absorption processes are present. Samples were measured as suspensions in a liquid cell with quartz (transient absorption experiments) or CaF_2 (infrared experiments) windows. All the transient absorption measurements were carried out using pump-probe methodology.

Nanosecond transient absorption kinetics were recorded by a frequency tripled Q-switched Nd:YAG laser coupled with a OPO (Quantel Brilliant B) to obtain the desired wavelength for the pump light (5 ns pulse at 10 Hz). A detection system from Applied Photophysics (LKS80 Spectrometer) was used, equipped with a Xe arc lamp (pulsed or continuous wave), two monochromators and a R928-type PMT read by an 600 MHz oscilloscope (Agilent Technologies Infinium 10 GSa/s) for kinetics. The kinetics were collected with the maximum resolution producing a 20000 points traces that were logarithmic oversampled starting from 50 points from the excitation about 10 ns after the pulse. The excitation light wavelength was chosen to be at the maximum of the absorption of the ZnO (355 nm). The excitation light power was controlled by mean of neutral density filters.

For ns transient infrared absorption measurements we used the same Q-switched Nd:YAG laser (Quanta-Ray ProSeries, Spectra-Physics) to obtain 532 nm pump light, 10 mJ/pulse with a FWHM of 10 ns. Probing was done with a continuous wave quantum cascade (QC) IR laser with a tuning capability between 1765-1925 cm^{-1}. For IR detection a liquid nitrogen-cooled mercury-cadmium-telluride (MCT) detector (KMPV10-1-J2, Kolmar Technologies, Inc,) was used. Transient absorption traces were acquired with a Tektronix TDS 3052 500 MHz (5GS/s) oscilloscope in connection with the L900 software (Edinburgh Instruments) and processed using Origin 9 software.

Femtosecond transient absorption infrared spectroscopy was carried out in a femtosecond transient absorption spectrometer (Helios IR, Ultrafast Systems LLC) at room temperature. A one- box Ti:Sapphire based amplifier with integrated oscillator and pump lasers (800 nm, 40 fs, 3 kHz, Libra LHE, Coherent Inc.) was used to pump two TOPAS Primes coupled with frequency mixers (Light Conversion Ltd) to produce the depolarized visible excitation and the broad mid-IR probe spectrum.

Time-resolved fluorescence measurements were performed with pump pulses generated via an optical parametric amplifier from 800 nm pulses with 250 fs, which were converted to 640 nm, and subsequently doubled to attain 320 nm with an OPO crystal. Fluorescence signals were measured with a streak camera with 5 ps resolution.

3. Results and discussion:

The high-resolution transmission electron microscope (HRTEM) micrographs show wurtzite type ZnO NCs as confirmed by Fast Fourier Transformation [12] performed on the selected 2D electron diffraction pattern of selected particles (SI Fig. S1). The measurements indicated that shape of the inorganic core of ZnO-OEG NCs was roughly spherical and crystalline with a mean diameter of 8.5 ± 1.2 nm (Fig. 1b; SI Fig. S1 and S2). The purity of crystal phase and the degree of crystallinity of ZnO-OEG NCs were further confirmed by powder X-ray diffraction (PXRD). The analysis of PXRD profile revealed well-defined reflexes, which were indexed to a single crystalline wurtzite structure of ZnO (SI Fig. S3). Based on the reflection broadening, according to the Williamson-Hall analysis, the crystallite size has been estimated to be 6.8 ± 0.6 nm. The average hydrodynamic diameter of ZnO-OEG NCs in water was 9 ± 2 nm as estimated using dynamic DLS (Fig. 1c, SI Fig. S4). Furthermore, in the FT-IR spectrum of ZnO-OEG NCs the intensive bands at 1434 and 1564 cm^{-1} characteristic for carboxylate (O−C−O) stretching modes are observed. This indicates that the carboxylic oligomers are anchored to the ZnO surface in the deprotonated form (Fig. S5). The resulting ZnO-OEG NCs remain stable in the solid state for months when stored under N_2 at 25°C.

Photophysical properties of ZnO-OEG NCs in water were determined by steady state absorption and emission upon band gap excitation. The material shows the characteristic absorption of ZnO NCs with a band gap at 373 nm (3.33 eV), depicted in Figure 2a [12]. The emission spectrum (excitation wavelength 355 nm) shows a small emission peak at around 404

nm (3.07 eV), and a pronounced emission at 560 nm (2.21 eV). The photoemission quantum yield at 560 nm was estimated to be 19.8% using Coumarine 343 in ethanol solvent as reference (63%) [13]. The emission at 404 nm relates to the recombination of electrons in a shallow trap located 0.26 eV below the conduction band with valence band hole [14]. The emission at 560 nm is from electrons in a shallow trap (0.26 eV below the conduction band) with deep trap holes at about 0.86 eV above the valence band edge (SI Fig. S13) [14]. We note, that the mentioned values correspond to the average minimum energy of the trap states, which are consistent to what has been published elsewhere [14]. Photophysical properties of ZnO-OEG NCs were essentially unchanged within minimum 7 days in water in a wide pH range (3-9) at 25°C, for details, see SI Fig. S6). We note, however, that the prolonged storage of ZnO-OEG NCs in water (over 3 days) led to a gradual self-assembly of the NCs and appearance of larger aggregates (as indicated by DLS measurements; SI Fig. S7), which resulted in slow decreasing of the absorption band intensity (SI Fig. S6).

Radiative recombination lifetimes of ZnO-OEG NCs were determined by time-resolved fluorescence spectroscopy (Fig. 2b and c). The experiments were carried out for a low concentration of the material and at excitation powers corresponding to less than one photon excitation per particle. Starting with emission at 404 nm, the signal decays within 25 ps, which is the maximum time for the electron trapping into the shallow trap states below the conduction band. The relative short lifetime is expected based on ZnO high electron mobility (Fig. 2b). The emission at 560 nm has significantly longer lifetimes, which precludes from measuring it with a streak-camera setup since the longest delay line that one can have is roughly 2 ns. Therefore, we have paid our attention to experiments conducted with a ns setup.

The experiment carried out with ns transient emission spectroscopy, following excitation with a single ~10 ns laser pulse, shows two clear emission components: a fast one and a slow one (Figure 2c). The trace could not be fitted with a simple sum of two exponentials due to the mismatching of the long component. A sum of a single exponential and a modified stretched exponential was necessary [15]. The fast component has a time constant of 34 ns (67%), the slow component has an average time constant of 2.2 μs (33%) and a β value of 0.56. The β value found here is slightly larger than typical β values present in literature for nanoscale interfacial electron transfer kinetics [16]. These photoluminescence decays measured for ZnO-OEG NCs obtained via organometallic approach were significantly longer than that typically observed for

ZnO nanoparticles. To the best of our knowledge, the longest biexponential photoluminescence decay with time constants of 1 and 14 ns was observed solely in good-quality ZnO single crystals prepared by physical methods [17]. For ZnO NCs with core-size in the *quantum size regime* the lifetimes were found to be between 25 and 30 ps for NCs with diameters of ca. 5.0, whereas for larger particles it was around 10 ps [14]. It is worth noting that the last family of NCs were derived from the classical inorganic sol-gel procedure [18], which provides ZnO nanostructures with inherently high sensitive core-organic shell interface towards the environment [10c]. Thus, the revealed long lifetimes for ZnO-OEG NCs nicely highlight the superiority of the organometallic wet-chemical process over the conventional sol-gel procedure as the effective method for the preparation of stable and well-passivated ZnO NCs. Moreover, in the case of these high-quality ZnO-OEG NCs, a particular charge stabilization mechanism must be present. It should be also mentioned, that the measured signal was almost the same in terms of charge lifetimes and components contribution when the measurement was performed in the absence of oxygen. Absence of dioxygen only led to an increase of the long-lived component contribution by ca. 5%. Furthermore, the fact that the time-resolved experiments are impervious to the presence of dioxygen in a solution at low sample concentration and excitation power indicates that charge stabilization mechanism is an intra-particle phenomenon.

There are three scenarios that can substantiate the observed charge stabilization mechanism, namely *(i)* electron stabilization; *(ii)* hole stabilization; or *(iii)* electron hole pair stabilization. To gain further insight into the charge stabilization mechanism, electron paramagnetic resonance (EPR) studies for the ZnO-OEG system were performed at 90 K and 298 K. Notably, the EPR spectra do not reveal the formation of persistent radical species for the sample measured in the dark and under UV irradiation, suggesting that charge carriers are not localized in a specific site in the inorganic core or the OEG shell.

Since the EPR measurements proved inconclusive, we employed for further investigations the ZnO NCs sensitized with betanin, ZnO-OEG-B NCs (Fig. 1a), a known organic dye capable of injecting electrons in ZnO conduction band upon excitation at 530 nm [19]. The adopted strategy offers two significant advantages, namely it provides the opportunity to study electron lifetime without the presence of the hole in ZnO, and confirms that the parent ZnO-OEG NCs can be post-synthetically modified with a dye, as conventionally done on dye-sensitized solar cells field. We opted to use betanin, a natural dye extracted from beetroot because it possesses –COOH

anchoring groups. We employed commercially available betanin, which displayed similar optical and femtosecond transient absorption behaviour as the one extracted from beetroot (SI Fig. S14) published elsewhere [20]. We note, that the observed change in betanin solution coloration upon addition of ZnO-OEG NCs is due to dye dilution (Fig. 1d) as confirmed by the optical measurements of the sensitized ZnO-OEG-B NCs. The affinity of betanin to ZnO surface was studied by ^{1}H NMR spectroscopy (SI Fig. S8).[21] In the ^{1}H NMR spectrum of the ZnO-OEG-B NCs signals attributed to the dye molecules became meaningfully sharpened in comparison to those observed for free betanin (SI Fig. S8) and these observations are consistent with the assumed interaction of betanine with the NCs surface. The further infrared measurements were performed in DMSO to prevent the large signal attenuation due to water bands. The electron lifetime in the ZnO-OEG-B system upon betanin excitation at 530 nm was monitored by ultrafast mid-infrared absorption spectroscopy (Fig. 3a; SI Fig. S15), which has an instrument response time of ca. 200 fs. It should be mentioned that free charge carriers yield a broad mid-infrared absorption originated from the metallic state [22]. Therefore, the detection of transient absorption upon betanin excitation is a direct measure of electron concentration in the ZnO conduction band, injected from the dye. The transient mid-infrared spectra show Drude behaviour (SI Fig. S15), although in our case considering the narrow range of energies probed (1850-2200 cm^{-1}), it is difficult to clearly observe such a dependence of the energies versus the intensity [23]. The kinetic trace extracted at 1897 cm^{-1} has two distinct rising edge components (1.3 and 14.0 ps) that are longer than the instrument response function. The rising edges are associated to the electron injection time (Fig. 3).

Recently, Knorr et al. demonstrated that electronically excited betanin is capable of two-electron injection into TiO_2 upon single photon absorption [19]. However, alternative explanations in decent order of likelihood are injection from different ZnO polarity surfaces and betanin surface coverage heterogeneity. However, the unequivocal interpretation of the two distinct rising edges is out of the scope of this study.

The measured mid-infrared absorption signal for ZnO-OEG-B NCs displays almost no decay within the experimental delay line (ca. 2 ns), suggesting long lifetimes of the order of tenths of ns as with the nanosecond experiment upon band gap excitation. In order to better estimate electron lifetime, ns time-resolved mid-infrared absorption experiments were performed. Figure 3b depicts the kinetic trace extracted at 2050 cm^{-1} from ns time-resolved mid-infrared absorption

experiments for ZnO-OEG-B NCs upon excitation at 532 nm. The signal was fitted with two exponential decays, namely fast component with a time constant of 1.5 μs (84%) and a slow component has an average time constant of 20.6 μs (16%). The offset in the spectra (roughly 15% of the total signal) is associated to the long-lived electrons that remain in the conduction band up to seconds, as depicted in the insets of Fig. 3b and 3c. Since the injected electron remains in the conduction band and survives for at least a couple of seconds, one can say that charge stabilization mechanism must be associated to hole stabilization and it is reasonable to assume that occurs within the OEG shell. The absence of a detectable EPR signal suggests that the hole is delocalized within the shell before it gets trap above the valance band. This mechanism has been proposed before for PEG-functionalized carbon nanotubes [24]. This is further corroborated by the time constants estimated from ns time-resolved mid-infrared absorption for direct band gap excitation, also depicted in Fig. 3c. Kinetic trace extracted at 2050 cm^{-1} from ns time-resolved mid-infrared absorption experiments for ZnO-OEG NCs upon excitation at 355 nm was fitted with two exponential decays, with a fast component with a time constant of 1.2 μs (91%) and a slow component has an average time constant of 15.1 μs (9%), which is very similar to the results for ZnO-OEG-B NCs. However, further work must be carried out in order to ascertain the mechanism and hole prime location. Notably, in both cases electrons survived in the conduction band up to seconds (insets of Fig. 3b and 3c), which opens the perspective of using the system for solar fuel production. Figure 4 summarizes the processes and associated time constants.

4. Conclusion:

In conclusion, we reported the first stable and water-soluble carboxylate oligoethylene glycol functionalized ZnO nanocrystals with slow back electron transfer dynamics (up to microseconds), which is related to hole stabilization. The material is a core-shell system with an almost impermeable OEG that can however be sensitized a posteriori. This is a necessary procedure in one wants to shift material light absorption to the visible range. To the best of our knowledge, the longest bi-exponential photoluminescence decay with time constants of 1 and 14 ns was observed solely in good-quality ZnO single crystals prepared by physical methods. For ZnO NCs with core-size in the *quantum size regime* the lifetimes were found to be between 25 and 30 ps for NCs with diameters of ca. 5.0, whereas for larger particles it was around 10 ps. The

properties of ZnO-OEG NCs circumvent all the known disadvantages, which precluded its large-scale use in n-type solar applications. It is our conviction that this material surpasses the commonly used n-type TiO_2 since electrons were found to survive in the semiconductor conduction band up to seconds, which at least four to six orders of magnitude of what as been reported for classical metal oxides nanoparticles, making it a new dawn for n-type dye sensitized solar cells and solar fuel devices. It should be emphasized that this is work is on its embryonic stage and the aim of this manuscript is to show the properties of our newly sensitized water stable ZnO NCs, not device fabrication. The addition of a dye was only to show that the nanomaterial could be functionalized and probe which of the charges gets stabilized.

Acknowledgements:

The authors would like to thank Uppsala University and The Knut and Alice Wallenberg Foundation for financial support. A. M. Cieślak, K. Sokołowski and J. Lewiński have received funding from the European Union's Horizon 2020 research and innovation Program under the grant agreement No 687008 (GOTSolar). J. Sá would like to acknowledge the Swedish Research Council (VR grant no. 2015-03764) for the financial support.

Figures:

Figure 1. a) Schematic representation of functionalization of ZnO-OEG NCs with betanin; b) HRTEM micrographs of ZnO-OEG NCs; (c) size distribution of ZnO-OEG NCs in water estimated by DLS; d) optical photograph depicting adsorption of betanin on the ZnO-OEG NCs surface: *(left)* betanin in DMSO and *(right)* betanin in DMSO after addition of ZnO-OEG NCs.

Figure 2. a) Steady absorption and photoluminescence upon excitation at 355 nm of ZnO-OEG NCs in aqueous solution; b) kinetic trace at 404 nm with streak camera time-resolved fluorescence upon excitation at 320 nm of ZnO-OEG NCs in aqueous solution in insert; c) kinetic trace at 560 nm measured with nanosecond time-resolved fluorescence upon excitation at 355 nm of ZnO-OEG NCs in aqueous solution and selected spectra at different times in insert.

Figure 3. a) Kinetic trace at 1897 cm^{-1} extracted from transient mid-infrared absorption spectra collected from 1850-2200 cm^{-1} of ZnO-OEG-B and ZnO-OEG NCs, and betanin upon excitation at 530 nm in DMSO. The insert depicts the two-rising edges functions for ZnO-OEG-B NCs with a time longer than instrument response function (ca. 100 fs); b) kinetic trace at 2050 cm^{-1} extracted from ns time-resolved mid infrared absorption spectra collected from 1850-2200 cm^{-1} of b) ZnO-OEG-B NCs (excited at 532 nm) and c) ZnO-OEG NCs (excited at 355 nm) in a DMSO.

Figure 4. Schematic representation of charge transfers processes and associated time constants on the ZnO-OEG-B system.

Figure 1:

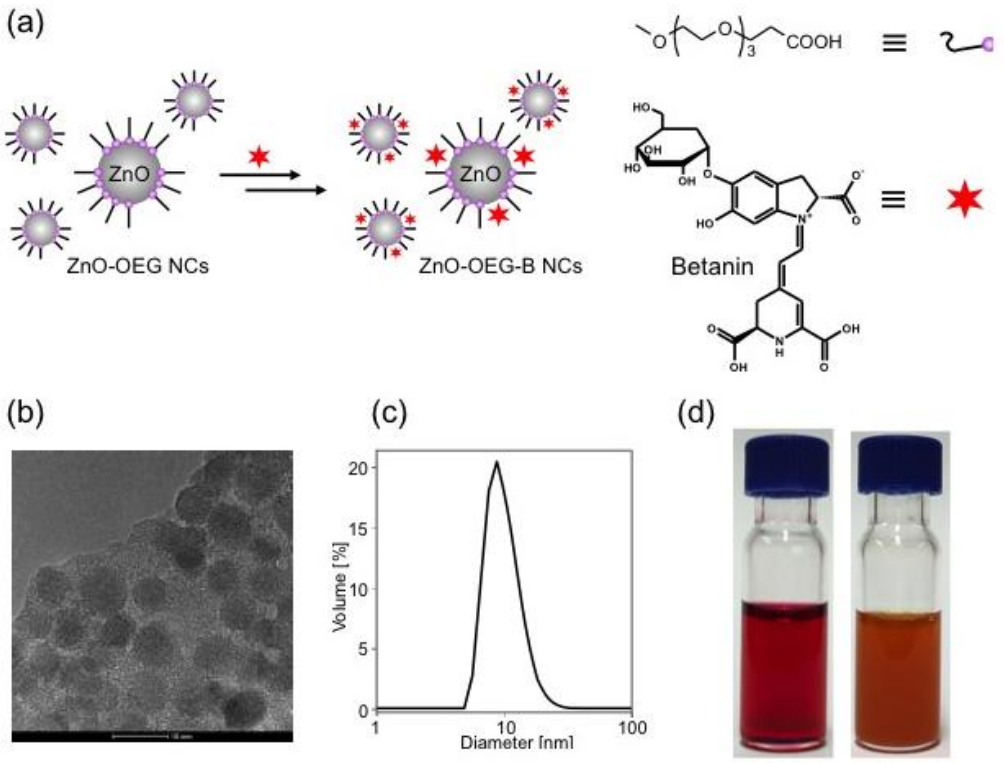

Figure 2:

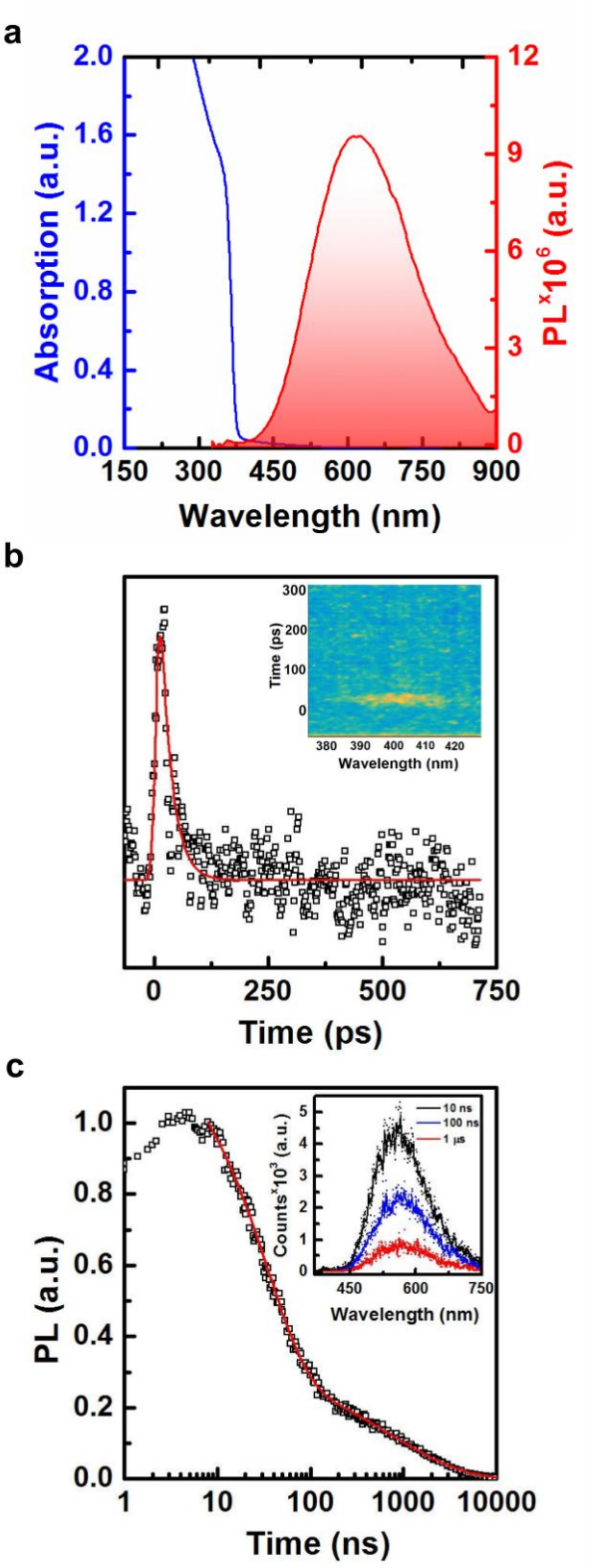

Figure 3:

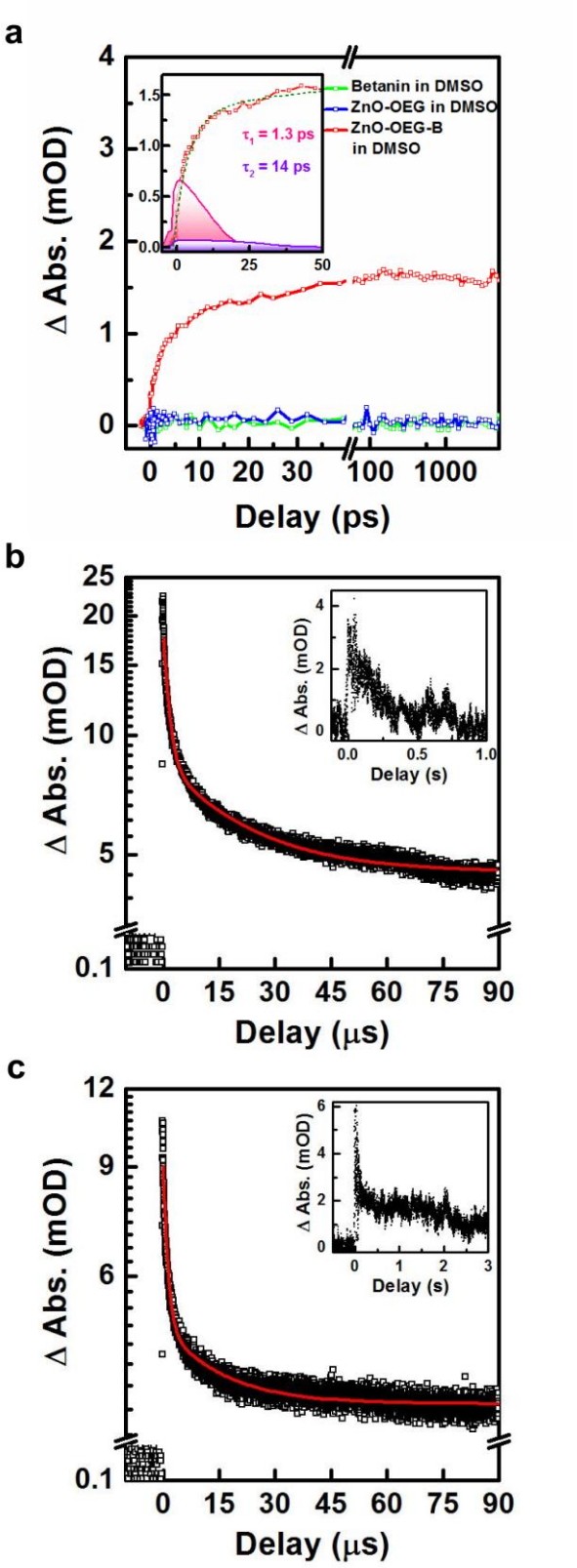

Figure 4:

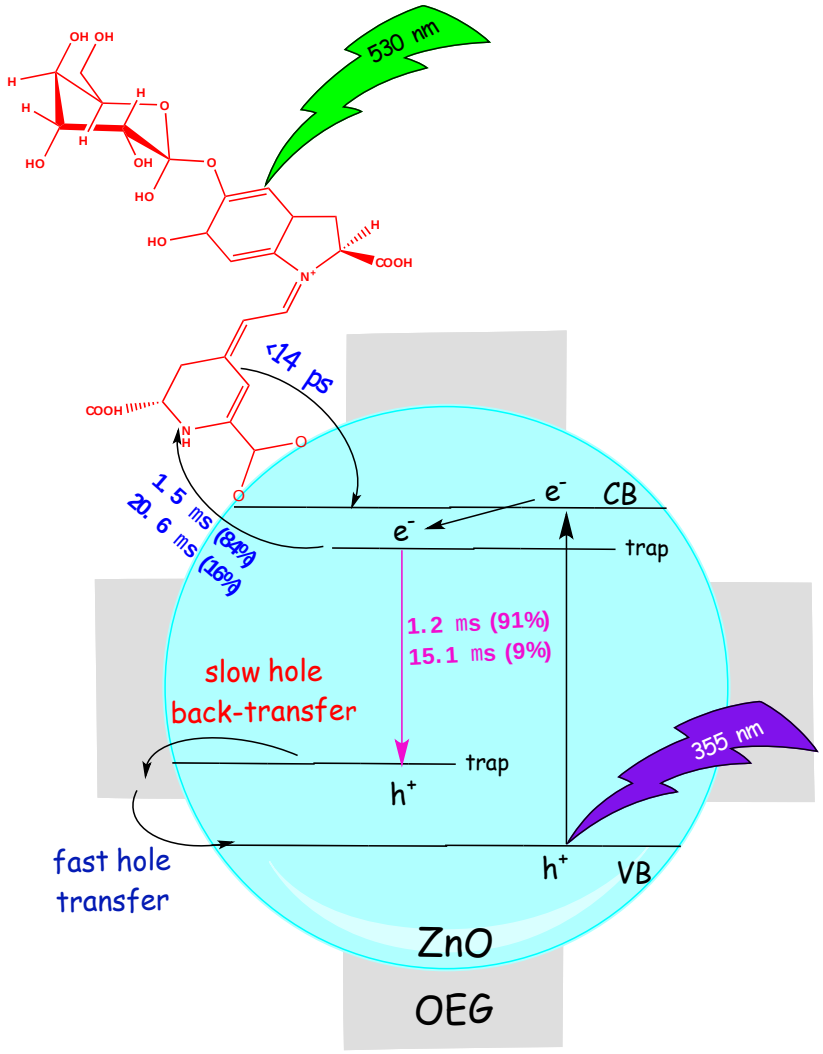

References:

[1] A. Listorti, B. O'Regan, J. R. Durrant, Chem. Mater. 23 (2011) 3381-3399

[2] O. Bräm, A. Cannizzo, M Chergui, Phys. Chem. Chem. Phys. 14 (2012) 7934-7937.

[3] A. Hagfeldt, M. Grätzel, Chem. Rev. 95 (1995) 49-68.

[4] M. Grätzel, Nature 414 (2001) 338-344.

[5] A. K. Chandiran, M. Abdi-Jalebi, M. A. Nazeeruddin, M. Grätzel, ACS Nano 8 (2014) 2261-2268.

[6] a) Y.-W. Jun, J.-S. Choi, J. Cheon. Angew. Chem. Int. Ed. 45 (2006) 3414-3439; b) S. Maiti, S. Pal, K. K. Chattopadhyay, CrystEngComm 17 (2015) 9264-9295.

[7] a) L. Guo, S. Yang, C. Yang, P. Yu, J. Wang, W. Ge, G. K. L. Wong, Appl. Phys. Lett. 76 (2000) 2901; b) H.-M. Xiong, J. Mater. Chem. 20 (2010) 4251-4262.

[8] J. Moser, M. Grätzel, J. Am. Chem. Soc. 105 (1983) 6547-6555.

[9] H.-M. Xiong, D.-P. Xie, X.-Y. Guan, Y.-J. Tan, Y.-Y. Xia, J. Mater. Chem. 17 (2007) 2490-2496.

[10] a) J. Paczesny, M. Wolska-Pietkiewicz, I. Binkiewicz, Z. Wróbel, M. Wadowska, K. Matuła, I. Dzięcielewski, D. Pociecha, J. S. Koziorowska, J. Lewiński, R. Hołyst, Chem. Eur. J. 21 (2015) 16941-16947; b) J. Paczesny, M. Wolska-Pietkiewicz, I. Binkiewicz, M. Wadowska, Z. Wróbel, K. Matuła, W. Nogala, J. Lewiński, R. Hołyst, ACS Appl. Mater. Interfaces 8 (2016) 13532–13541; c) A. Grala, M. Wolska-Pietkiewicz, W. Danowski, Z. Wróbel, J. Grzonka, J. Lewiński, Chem. Comm. 52 (2016) 52, 7340-7342; d) A. M. Cieślak, E.-R. Janeček, K. Sokołowski, T. Ratajczyk, M. K. Leszczyński, O. A. Scherman, J. Lewiński, Reversible light modulation of cucurbit[8]urils host−guest systems through photoactive water-soluble ZnO nanocrystals, submitted to Angewandte Chemie no. 201604116.

[11] a) L. C. P. Gonçalves, S. M. Silva, P. C. DeRose, R. A. Ando, E. L. Bastos, Plos One, 8 (2013) e73701; b) L. C. P. Gonçalves, R. R. Tonelli, P. Bagnaresi, R. A. Mortara, G. A. Ferreira, E. L. Bastos, Plos One 8 (2013) e53874.

[12] a) J. N. Schrauben, R. Hayoun, C. N. Valdez, M. Braten, L. Fridley, J. M. Mayer, Science 336 (2012) 1298-1301; b) M. N. Braten, D. R. Gamelin, J. M. Mayer ACS Nano 2015, 9, 10258-10267.

[13] G. A. Reynolds, K. H. Drexhage, Opt. Commun. 13 (1975) 222-225.

[14] T. J. Jacobsson, S. Viarbitskaya, E. Mukhtar, T. Edvinsson, Phys. Chem. Chem. Phys. 16 (2014) 13849-13857.

[15] M. Berberan-Santos, E. Budunov, B. Valeur, Chem. Phys. 315 (2005) 171-228.

[16] a) J. Nelson, S. A. Haque, D. Klug, J. R. Durrant, Phys. Rev. B. 63 (2001) 205321; b) A. N. Green, E. Palomares, S. A. Haque, J. M. Kroon, J. R. Durrant, J. Phys. Chem. B 109 (2005) 12525-12533; c) L. D'Amario, L. Antila, B. P. Rimgard, G. Boschloo, L. Hammarström, J. Phys. Chem. Lett. 6 (2015) 779-783.

[17] Y. Zhong, A. B. Djurišić, Y. F. Hsu, K. S. Wong, G. Brauer, C. C. Ling, W. K. Chan, J. Phys. Chem. C 112 (2008) 16286-16295 and references therein.

[18] a) L. Spanhel M. A. Anderson, J. Am. Chem. Soc. 113 (1991) 2826-2833; b) E. A. Meulenkamp, J. Phys. Chem. B 102 (1998) 5566-5572.

[19] F. J. Knorr, J. L. McHale, A. E. Clark, A. Marchioro, J.-E. Moser, J. Phys. Chem. C 119 (2015) 19030-19041.

[20] M.Wendel, S, Nizinski, D. Tuwalska, K. Starzak, D. Szot, D. Prukala, M. Sikorski, S. Wybraniec, G. Burdzinski, Phys. Chem. Chem. Phys. 17 (2015) 18152-18158.

[21] The FTIR spectra were inconclusive on this occasion due to the bands overlap of the carboxylate groups of oligoethylene glycol ligand and betanin (SI Fig. S5).

[22] a) H. Matsuzaki, Y. Matsui, R. Uchida, H. Yada, T. Terashige, B. S. Li, A. Sawa, M. Kawasaki, Y. Tokura, H. Okamoto, J. Appl. Phys. 115 (2014) 053514; b) P. Friedli, H. Sigg, J. Sá, Photochem. Photobiol. Sci. 13 (2014) 1393-1396; c) J. Sá, P. Friedli, R. Geiger, P. Lerch, M. H. Rittmann-Frank, C. J. Milne, J. Szlachetko, F. G. Santomauro, J. A. van Bokhoven, M. Chergui, M. J. Rossi, H. Sigg, Analyst 138 (2013) 1966-1970.

[23] L. J. Antila, F. G. Santomauro, L. Hammarström, D. L. A. Fernandes, J. Sá, Chem. Commun. 51 (2015) 10914-1916.

[24] L. Cao, S. Sahu, P. Anilkumar, C. E. Bunker, J. Xu, K. A. S. Fernando, P. Wang, E. A. Guliants, K. N. Tackett, II; Y. P. Sun, J. Am. Chem. Soc. 2011, 133, 4754-4757.